A light-in-flight single-pixel camera for use in the visible and short-wave infrared

Steven D. Johnson,[1,*] David B. Phillips,[2] Zelin Ma,[3] Siddharth Ramachandran,[3] and Miles J. Padgett[1]

[1] SUPA, University of Glasgow, School of Physics and Astronomy, Glasgow, UK
[2] University of Exeter, School of Physics, Exeter, UK
[3] Boston University, 8 St. Mary's St, Boston, Massachusetts 02215, USA
*steven.johnson@glasgow.ac.uk

Abstract: Single-pixel cameras reconstruct images from a stream of spatial projection measurements recorded with a single-element detector, which itself has no spatial resolution. This enables the creation of imaging systems that can take advantage of the ultra-fast response times of single-element detectors. Here we present a single-pixel camera with a temporal resolution of 200 ps in the visible and short-wave infrared wavelengths, used here to study the transit time of distinct spatial modes transmitted through few-mode and orbital angular momentum mode conserving optical fiber. Our technique represents a way to study the spatial and temporal characteristics of light propagation in multimode optical fibers, which may find use in optical fiber design and communications.

1. Introduction

Conventional cameras record images using pixelated sensor arrays. In contrast, single-pixel imaging enables images to be reconstructed using a single-element detector such as a photodiode. In this approach different regions of a scene are sequentially masked, and the single-pixel detector measures the correlation of the scene with each masking pattern. Post-processing of these measurements enables an image of the scene to be reconstructed [1–4], by recording the change in signal over time for each pattern a temporally changing picture can be reconstructed. The use of a single-pixel detector enables images to be recorded at wavelengths where conventional camera sensors do not exist, such as in the THz band [5–7], and the temporal response can vastly exceed that of conventional camera sensors.

Here we exploit the ultra-fast response times of single-element detectors to image light-in-flight, we apply the technique to directly observe the spatial and temporal evolution of light propagating through multimode optical fibers (MMFs). Single-pixel imaging provides a complementary approach to previously demonstrated ultra-fast imaging techniques, such as those relying on single-photon avalanche diode (SPAD) arrays, streak cameras or gated intensified charged coupled devices (ICCD) [8–12]. SPAD detectors measure the arrival time of single photons with high temporal resolution, by combining individual SPAD detectors into an array a camera with spatial resolution is created. These SPAD arrays have excellent timing resolution, between 50 ps to 200 ps, and have been created with up to 256×256 pixels [9]. Streak cameras have been shown to produce very fast images, with exposure times of 10 ps for one-dimensional or compressed sensing measurements. Timing resolution for ICCD systems range from a few nanoseconds to 200 ps by using an intensifier as a shutter to briefly expose the CCD, this produces a large pixel array that is capable of single-photon imaging. As these methods rely on silicon detectors, they have no sensitivity to photon wavelengths outside of the visible and near-infrared. Although short-wave infrared (SWIR) single-element SPAD detectors are commercially available, no SPAD array has been created that is sensitive at telecommunications wavelengths. Detectors that are sensitive outside of the visible spectrum can be very expensive, and the cost of fabrication
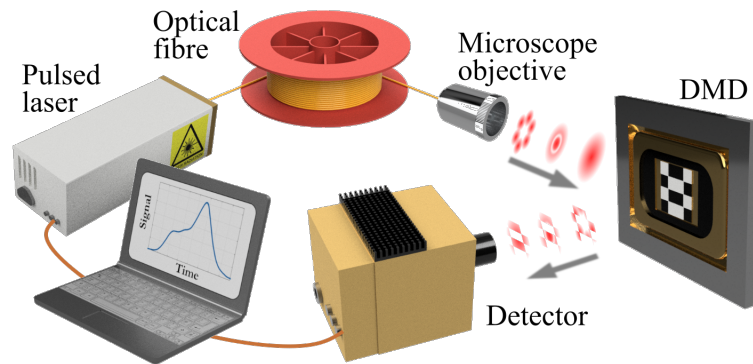
Fig. 1. The experimental set-up of our light-in-flight camera system. A pulsed supercontinuum laser illuminates the input to the optical fiber under test. The illumination wavelength is selected with a bandpass filter within the laser assembly (not shown). Light exiting from the output of the optical fiber is collected by a microscope objective and transmitted to a digital micro-mirror device (DMD), displaying a series of mask patterns. The light reflected from the *on* mirrors of the DMD is transmitted to the single-pixel detector. The photon arrival time is measured by the time correlated single-photon counting (TCSPC) electronics, timed with respect to an electronic synchronisation signal from the laser controller.

for pixelated-arrays is much greater than producing a single-element detector. Because of this relatively cheap cameras can be made using single-pixel imaging. The single-pixel imaging system presented here represents a comparatively simple method to achieve high temporal resolution light-in-flight imaging.

Optical fibers have become ubiquitous in communications infrastructure, the accelerating global demand for telecommunications has propelled research into increasing the transmission capacity of optical fibers. Multiplexing has been performed in time, wavelength, polarisation and phase; but the physical limits of a single-mode optical fiber are now restricting further improvement using these degrees of freedom alone [13, 14]. Research is now focused on utilising the spatial dimension to increase information capacity, one option is to take advantage of optical fibers that inherently support multiple spatial modes that can act as parallel channels of information transmission [15–17].

Waveguide theory provides a variety of models describing how light propagates through ideal MMFs [18, 19]. The spatial modes supported by a lossless MMF form an orthogonal set of 2D monochromatic complex field distributions, each described by a specific intensity and phase pattern at a given wavelength and polarisation. For a conventional optical fiber the modes are weakly guided in the core, the transverse components of the electric field are much larger than the longitudinal components thereby having a distinct spatial distribution, known as linearly polarised (LP) modes. An LP mode is described by the indices l and m characterising its azimuthal and radial distributions respectively, usually denoted as LP_{lm} mode. In the case of an ideal optical fiber (perfectly straight with cylindrical symmetry) these spatial modes maintain the same intensity cross-section at any axial point along the fiber.

Optical fibers have the property of modal dispersion, due to lower-order modes travelling with a higher group velocity than the higher-order modes, such that modes in a short pulse of light launched into the optical fiber simultaneously will be emitted at different times. As pulse separation is linearly proportional to fiber length, with sufficiently long fiber and a detector with high temporal resolution, the light propagating in each spatial mode will be separated by a large enough time interval that distinct pulses can be measured. How the light is coupled into the optical fiber determines which modes are transmitted, the complex spatial overlap between the

input beam shape and the spatial modes supported by the fiber determines which modes of the MMF are excited, and the excitation groups can be varied by adjusting the coupling of the laser source into the optical fiber.

In general, the transmission characteristics of light in a real optical fiber depart from those predicted due to bends and twists, fabrication tolerances, index variations along the fiber length and temperature variations [20]. Even very subtle differences from theory can quickly yield large observed changes in transmission dynamics. While the underlying theory of ideal MMFs is well established, understanding the full range of propagation characteristics exhibited by real-world fibers, and how to best mitigate unwanted deviations through design and use, is still a subject of active investigation. By measuring the effects bending has on a MMF these perturbations can be predicted and corrected for [21, 22].

The existing techniques for measuring optical fiber modes such as spatial and spectral reconstruction, S^2 [23], and cross-correlated imaging, C^2 [24], require interference measurements and complex algorithms to extract the temporal and spatial information. The techniques use spectral interference between the different modes within an optical fiber, whereas our single-pixel technique is a measurement of the system using a direct temporal measurement. Single-pixel imaging schemes acquire a sequence of measurements in a multi-shot process, a method well suited for analysis of the spatial and temporal evolution of pulsed light repeatedly transmitted through static optical fiber. Here we perform measurements at both visible and SWIR, at the telecommunications wavelength 1550 nm. The single-pixel camera does not require any optics or complex set up to change between different detectors for different wavelength ranges, this versatility enables the camera to be easily adapted for new field of study. The advantage of our system is the SWIR sensitivity that conventional streak camera and ICCD do not have, as silicon is not sensitive at telecommunications wavelengths.

In this work we apply a temporally resolved single-pixel camera, operating with a temporal resolution of 200 ps, to observe the transit of light pulses propagating through multimode fibres. This allows direct observation of the transit time of different spatial mode groups supported by the fibers. We first demonstrate proof-of principle measurements on a stepped index few-mode fibre in the visible region of the spectrum. Next, by replacing the visible detector with a short wave infra-red counterpart, we switch our system to operate in the SWIR telecommunication band, and use it to measure mode group transit time through an orbital angular momentum (OAM) conserving air-core fiber.

2. Single-pixel camera design

The single-pixel measurement is made by sampling the emitted light from an optical fiber with a variable mask set and measuring the temporal signal. Figure 1 shows a schematic of our optical fiber and single-pixel imaging set up. A pulsed supercontinuum laser (Fianium SC-400, pulse frequency 60 MHz, pulse length 6 ps) illuminates the input to the optical fiber under test, the wavelength is selected with a bandpass filter at the laser output. Light exiting from the output of the optical fiber is collected by a microscope objective (Olympus ×20, 0.5 NA) and transmitted 50 mm through free-space to a digital micro-mirror device (DMD). A DMD is an array of tiltable mirrors, by displaying a pattern on the DMD the mirrors tilt to selects if the light for each spatial position is be directed towards the detector or away to a beam dump. The DMD (ViALUX V-7001) has 1024 × 768 mirrors with a 13.7 μm pitch. The single-pixel detector measures the total intensity transmitted through the DMD mask as a function of time, which constitutes a measurement of the level of correlation between the incident light field from the optical fiber and the mask pattern displayed on the DMD. The time varying signal is measured using a photon-counting single-pixel detector with a very fast response time. Using the technique of time correlated single-photon counting (TCSPC), the electronics (PicoQuant TimeHarp 260, time-bin width 25 ps) produce a histogram of the arrival times of single-photon events from the detector

with respect to a synchronisation pulse from the laser. This implementation of the single-pixel technique has been used previously for 3D imaging applications [25, 26]. The reconstruction from the single-pixel image is performed for the data at each time-bin, by considering each time-bin to be an individual frame in the video the mode image can be reconstructed for that point in time. The time-bin width is 25 ps but the limitation on our measurement is the temporal response of the detector used.

To fully sample the light field, we must acquire measurements for the number of patterns that is equal to, or greater than, the number of pixels in the final reconstructed image. A variety of different pattern sets have been previously demonstrated, such as those drawn from the Fourier basis or Hadamard basis [27, 28]. The Hadamard basis is the simplest to implement using a DMD as the patterns are binary in nature, they are an orthogonal set of patterns where half the signal is measured for any one pattern. The Hadamard pattern set comprises of elements taking the value of +1 or -1, but a DMD can only modulate the intensity by a factor of 1 or 0. To perform a measurement with the Hadamard patterns the signal is measured for the positive pattern (the +1 values are displayed on the DMD) and then for the negative pattern (the -1 values pattern are displayed); the negative histogram is subtracted from the positive histogram to give the temporal measurement for the respective Hadamard pattern. The intensity at each time-bin $M(t)_i$ is then used to compute a spatial image $I_{2D}(t)$ by performing a weighted sum of each of the Hadamard patterns H_i, each weighted by its measured level of correlation. The image is reconstructed as

$$I_{2D}(t) = \sum_{i=1}^{N} M(t)_i \cdot H_i, \tag{1}$$

where N is the number of Hadamard patterns, also corresponding to the number of pixels in the reconstructed image. This yields a 3D data-set capturing how the 2D image signal varies with time.

The detectors used have very low dark signal, the shot noise is the dominant noise in the single-photon counting measurement. Many single-photon detections are spread over the time-bins of our histogramming TCSPC system, such that some time-bins contain very little signal. To reduce the impact of the high signal-to-noise in our images we used a 3D smoothing kernel to suppress the noise spatially in the x and y spatial dimensions and temporal dimension t; with the assumption that the measured image is changing relatively slowly in both space and time, in comparison with the pixel and temporal resolution of the measurement. The smoothing kernel uses a Gaussian distribution-shape kernel of the form

$$K(x, x', y, y', t, t') = \exp\left(\frac{-(x-x')^2}{2\sigma_{xy}^2}\right) \cdot \exp\left(\frac{-(y-y')^2}{2\sigma_{xy}^2}\right) \cdot \exp\left(\frac{-(t-t')^2}{2\sigma_{t}^2}\right) \tag{2}$$

with a spatial spread of $\sigma_{xy} = 1$ pixel, and a temporal spread equal to approximately half the detector jitter, $\sigma_{t} = 4$ time bins. The smoothed image $Y(x, y, z)$ is calculated from the original image $X(x, y, t)$ as

$$Y(x', y', t') = \iiint K(x, x', y, y', t, t') \cdot X(x, y, t) \, dx \, dy \, dt. \tag{3}$$

As smoothing was performed in the spatial and temporal dimensions many pixels contribute to each pixel's value. To reduce the measurement noise an alternative compressive sensing technique could have been used, such as optimisation of the reconstruction based on image sparsity [3], however this method did not give better results in our experience.

3. Few-mode optical fiber measurement

The single-pixel system was used to view the modes of a few-mode optical fiber (FMF). The optical fiber under test was a 50 m long stepped-index optical fiber (numerical aperture of 0.14,
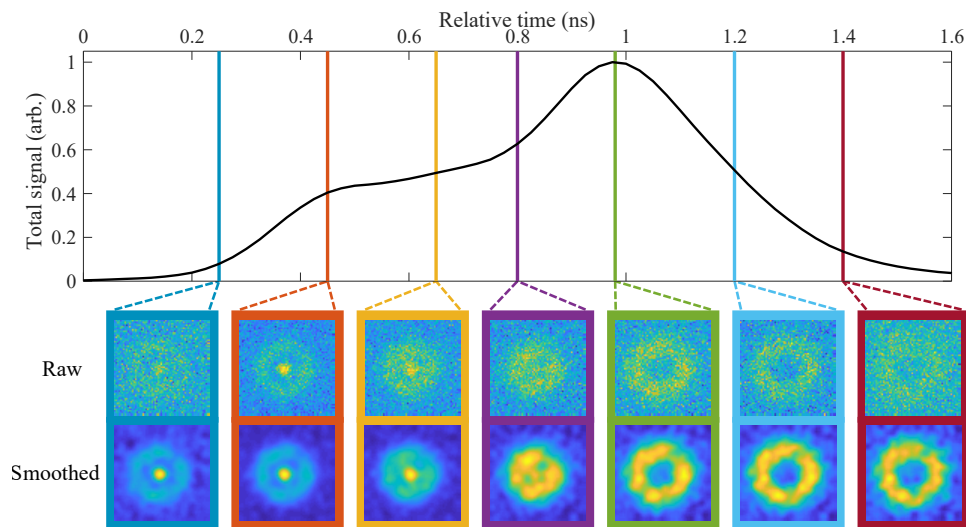
Fig. 2. The upper plot shows the total intensity transmitted from the FMF as a function of time, calculated by summing the contributions from all patterns. The normalised 2D intensity distribution at several different times are shown below, with the raw image and the image after kernel smoothing, the line colour corresponds to the time of the image frame shown. The images of the modes have been normalised giving each image the maximum contrast. The full data is shown in Visualization 1.

core diameter of ~5.8 μm) designed to be single-mode at wavelengths longer than 980 nm. By operating the fiber at wavelengths shorter than this cut-off several modes are supported, making it a FMF. To select the laser wavelength a bandpass filter with a central wavelength of 450 nm and a bandwidth of 6 nm was used. The Gaussian mode emitted from the laser was coupled into the optical fiber via a microscope objective. By the deliberate misalignment of the fiber coupler the Gaussian excitation field was offset with respect to the optical fiber axis, increasing the correlation of the excitation field with the higher order modes.

The single-pixel detector used for the visible light experiment was a photo-multiplier tube (PMT) in photon-counting Geiger mode. The detector had a timing precision full-width half maximum of 180 ps (detector jitter) and a 10 mm^2 active area (PicoQuant PMA 192). Photon-counting detectors exhibit a period of dead time after each detection, during which they cannot detect photons. If the incident photon flux is too high, this can lead to a bias towards earlier regions of the measured histograms. This detection issue can be resolved by limiting the detection flux to around 5% of the maximum detection rate. Hence, the average detection rate using our PMT was 5×10^6 photons per second. A 64×64 image was captured requiring 8192 mask patterns, the signal for each pattern was measured for 1 second, and the total acquisition time was approximately 2.5 hours.

Figure 2 show a series of snapshots depicting how the field intensity of a pulse exiting the FMF evolves over the course of 1.6 ns. The optical modes are separated simply by the modes travelling with different group velocities within the FMF. We observe three distinct field intensity patterns emanating from the FMF, these are recognised as low-order LP$_{lm}$ modes but it's not possible to determine from our measurement exactly which modes are present. Visualization 1 shows the full time-series for our measurement displaying the modal evolution of the FMF output. Tests were performed where optical fiber was contorted and the modes were measured, no obvious changes in the mode pattern were seen due to bending. Mode coupling by changing the optical input to the fiber did change the mode patterns, this is shown in Visualization 2

where a different mode-coupling due to laser alignment has been produced (measured at 32×32 resolution). The contributing factor of our pulse broadening due to chromatic dispersion (using the Sellmeier equation [29]) was calculated to contribute 80 ps to the overall convolution of the mode broadening. The chromatic dispersion is smaller than the detector jitter of 180 ps, and hence, the jitter of the PMT detector is the largest contributor to the signal spread that would limit our temporal resolution.

4. OAM optical fiber measurement

The amplitude of a Laguerre-Gaussian mode has an azimuthal angular dependence of $\exp(il\phi)$, where l is the azimuthal mode index, these modes have a well-defined orbital angular momentum L that has a value of $l\hbar$ per photon [30]. The helicity of the optical beam is quantized such that the angular momentum L is an integer, the radius of the beam intensity distribution increases with L [31]. Here we consider OAM modes that are characterised by having helical wavefronts that propagate carrying values of angular momentum L. Specialised optical fibers have been designed to support the transmission of OAM modes, air-core optical fibers have been shown to conserve the transmission of OAM modes over long distances with small cross-talk to other modes [32, 33]. As the air-core optical fiber has structure they no longer produce the classical LP modes, but the constrained modes are similar. The higher-order OAM modes travel with a smaller group velocity within the optical fiber. The OAM mode helicity direction can be defined with respect to the circular polarisation of the light, such that it can be spin-orbit aligned or spin-orbit anti-aligned; this is an important characteristic as it affects the propagation velocity of the mode. The previous work [32] has presented the propagation delay of the different order OAM modes, non-spatial time-of-flight measurements showed different spin-orbit modes propagate with different group velocities. By launching a single OAM mode into the optical fiber, the fidelity of the single-mode conservation was demonstrated by taking a measurement of the temporal signal, any cross-talk would be indicated by the arrival of photons at times other than the transmission time of the intended optical mode.

The single-pixel camera was used to measure the transmission of modes through the OAM fiber where multiple modes were excited simultaneously. The changes made to the system for the SWIR measurement were to use 200 m of the air-core fiber presented in [32] (radius of the air-core of 3 μm, outer radius of core of 8.25 μm) and the bandpass filter used had a wavelength of 1550 nm and a bandwidth of 12 nm. The PMT used for the FMF measurement was not sensitive in the infrared, instead a SWIR single-photon counting SPAD detector (IDQ230) was used, sensitivity in the range 900 nm to 1700 nm and a detector jitter of 220 ps. Coupling to the SPAD detector was via a short multimode optical fiber, to uniformly sample the spatial information without vignetting the image a ground glass plate was place in front of the detector input fiber to disperse the signal reflected from the DMD. The SWIR detection had a significantly lower detection rate compared to the visible wavelength PMT, the average detection rate was 1×10^5 photons per second. Hence a 32×32 resolution requiring 2048 mask patterns was used with a 5 second integration time per pattern and a total acquisition of 2.8 hours.

Figure 3 shows the temporal signal and the predicted transit times of the OAM modes. Visualization 3 shows the full time-series for our measurement with the OAM fiber. The propagation group velocity for each of the modes was predicted using the model detailed in [34], for our OAM fiber the propagation delay was calculated for the spin-orbit aligned mode. The dispersion measured is consistent with the results measured in [33] where modes were created and input into the optical fiber one at a time; our system has measured these modes simultaneously. Although the $|L| = 3$ peak maximum is observed to arrive before the predicted time, the modal spatial distribution is still correct. The difference in the propagation velocities of the spin-orbit aligned and spin-orbit anti-aligned modes becomes significant for the higher L modes, hence the $|L| = 5$ and $|L| = 6$ modes having temporally wider peaks due to the propagation difference
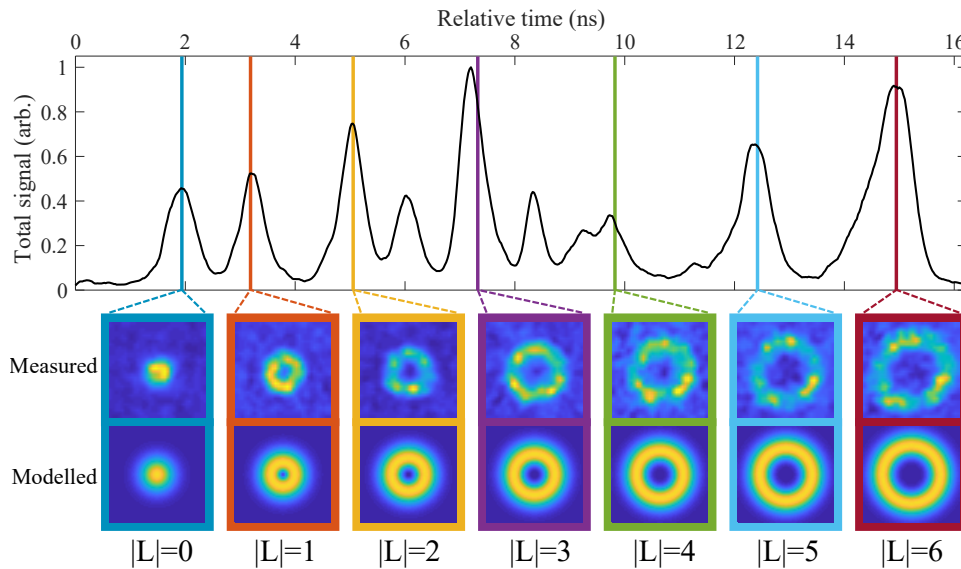
Fig. 3. The upper plot shows the integral intensity transmitted as a function of time from the 200 m length of OAM fiber. The vertical lines show the predicted arrival time of the optical modes. For each mode the measured intensity pattern and the respective modelled intensity of the OAM modes are shown. The unlabelled peaks in the plot are identified as higher order modes that were not included in the mode predictions. The images of the modes have been normalised giving each image the maximum contrast. The full data is shown in Visualization 3.

between the two contributing modes. The predicted difference in the time of transmission for the $|L| = 1$ modes is 7 ps, whereas for the $|L| = 6$ modes is 190 ps. The mode radius is shown to increase in size as the L increases, the predicted LP_{l1} modes associated with the OAM modes are shown below the measured image for each of the predicted arrival times, where $l = |L| + 1$. The additional peaks in the image are identified as LP_{l2} modes that were not included in the model predictions.

5. Conclusion

In this work we have demonstrated a single-pixel camera that is sensitive in the visible and SWIR with a temporal resolution of 200 ps. The camera has been utilised to image the temporal evolution of a pulse of light transmitted through a few-mode optical fiber and an OAM conserving optical fiber. The single-pixel camera uses the reflected signal from a DMD and a single-pixel detector to measure the temporal signal for each of the patterns displayed, from which the spatial patterns are calculated. Distinct intensity patterns that are associated to individual spatial modes with 200 ps temporal separation have been imaged with a visible single-pixel light detector. By using a detector sensitive in the SWIR the OAM modes of a specially constructed air-core optical fiber have been imaged at telecommunications wavelengths. The limitation on the temporal measurement is identified as the detector jitter in both cases, hence the measurement could be improved by using a different detector such as a SPAD detector that has smaller jitter or a superconducting nanowire single-photon detector where order of magnitude improvements in jitter have been shown [35, 36]. In addition to detectors with higher count rates, there are techniques that have been shown to improve the noise performance of single-pixel measurements [37], which could reduce the current substantial acquisition times.

The cost of a high-quality DMD is much cheaper than the difference between a single-element

detector and an array detector for the SWIR. However, a significant drawback is the acquisition time required for the measurement of each pattern shown on the DMD. As single-photon counting detectors are used here this significantly increases the time required to acquire the intensity signal compared to conventional optical sensors. There is also a maximum rate the patterns can be displayed on the DMD and the data acquired, this limits the resolution that can be used without the length of acquisition becoming prohibitive. As the technique required many repeat

This method of light-in-flight measurement has the advantage over SPAD arrays that the measurement can be performed at SWIR wavelengths, which would not be possible with normal silicon detectors. The single-pixel camera based technique we demonstrate in this work complements existing methods to study pulse transit through multimode fibres [32, 33]. Our technique provides different information: it gives the mode pulse intensity as a function of time rather than spectrally resolved complex field measurements. However our method avoids the need for interferometric stability and so is simpler to implement. Nonetheless, this approach could be extended to temporal complex field measurements by combing single-pixel intensity imaging with phase stepping holography.

Disclosures

The authors declare that there are no conflicts of interest related to this article.

References

1. A. Kirmani, D. Venkatraman, D. Shin, A. Colaço, F. N. C. Wong, J. H. Shapiro, and V. K. Goyal, "First-photon imaging," Science **343**, 58–61 (2014).
2. Y. Bromberg, O. Katz, and Y. Silberberg, "Ghost imaging with a single detector," Phys. Rev. A **79**, 053840 (2009).
3. M. F. Duarte, M. A. Davenport, D. Takhar, J. N. Laska, T. Sun, K. F. Kelly, and R. G. Baraniuk, "Single-pixel imaging via compressive sampling," IEEE Signal Process. Mag. **25**, 83–91 (2008).
4. S. S. Welsh, M. P. Edgar, R. Bowman, P. Jonathan, B. Sun, and M. J. Padgett, "Fast full-color computational imaging with single-pixel detectors," Opt. Express **21**, 23068–23074 (2013).
5. R. I. Stantchev, B. Sun, S. M. Hornett, P. A. Hobson, G. M. Gibson, M. J. Padgett, and E. Hendry, "Noninvasive, near-field terahertz imaging of hidden objects using a single-pixel detector," Sci. Adv. **2**, e1600190 (2016).
6. R. I. Stantchev, D. B. Phillips, P. Hobson, S. M. Hornett, M. J. Padgett, and E. Hendry, "Compressed sensing with near-field THz radiation," Optica **4**, 989–992 (2017).
7. L. Olivieri, J. S. Totero Gongora, A. Pasquazi, and M. Peccianti, "Time-resolved nonlinear ghost imaging," ACS Photonics **5**, 3379–3388 (2018).
8. D. Faccio and A. Velten, "A trillion frames per second: the techniques and applications of light-in-flight photography." Rep. Prog. Phys. **81**, 105901 (2018).
9. X. Ren, P. W. R. Connolly, A. Halimi, Y. Altmann, S. McLaughlin, I. Gyongy, R. K. Henderson, and G. S. Buller, "High-resolution depth profiling using a range-gated CMOS SPAD quanta image sensor," Opt. Express **26**, 5541–5557 (2018).
10. R. Warburton, C. Aniculaesei, M. Clerici, Y. Altmann, G. Gariepy, R. McCracken, D. Reid, S. McLaughlin, M. Petrovich, J. Hayes, R. Henderson, D. Faccio, and J. Leach, "Observation of laser pulse propagation in optical fibers with a SPAD camera," Sci. Rep. **7**, 43302 (2017).
11. G. Gariepy, N. Krstajić, R. Henderson, C. Li, R. R. Thomson, G. S. Buller, B. Heshmat, R. Raskar, J. Leach, and D. Faccio, "Single-photon sensitive light-in-fight imaging," Nat. Commun. **6**, 6021 (2015).

12. L. Gao, J. Liang, C. Li, and L. V. Wang, "Single-shot compressed ultrafast photography at one hundred billion frames per second," Nature **516**, 74–77 (2014).
13. D. J. Richardson, J. M. Fini, and L. E. Nelson, "Space-division multiplexing in optical fibres," Nat. Photonics **7**, 354–362 (2013).
14. R.-J. Essiambre and R. W. Tkach, "Capacity trends and limits of optical communication networks," Proc. IEEE **100**, 1035–1055 (2012).
15. S. Randel, R. Ryf, A. Sierra, P. J. Winzer, A. H. Gnauck, C. A. Bolle, R.-J. Essiambre, D. W. Peckham, A. McCurdy, and R. Lingle, "6×56-Gb/s mode-division multiplexed transmission over 33-km few-mode fiber enabled by 6×6 MIMO equalization," Opt. Express **19**, 16697–16707 (2011).
16. N. Bai, E. Ip, Y.-K. Huang, E. Mateo, F. Yaman, M.-J. Li, S. Bickham, S. Ten, J. Linares, C. Montero, V. Moreno, X. Prieto, V. Tse, K. M. Chung, A. P. T. Lau, H.-Y. Tam, C. Lu, Y. Luo, G.-D. Peng, G. Li, and T. Wang, "Mode-division multiplexed transmission with inline few-mode fiber amplifier," Opt. Express **20**, 2668–2680 (2012).
17. N. Bozinovic, Y. Yue, Y. Ren, M. Tur, P. Kristensen, H. Huang, A. E. Willner, and S. Ramachandran, "Terabit-scale orbital angular momentum mode division multiplexing in fibers," Science **340**, 1545–1548 (2013).
18. K. Okamoto, *Fundamentals of optical waveguides* (Academic Press, 2006).
19. B. E. A. Saleh and M. C. Teich, *Fiber Optics* (Wiley-Blackwell, 2001), chap. 8, pp. 272–309.
20. R. Olshansky, "Propagation in glass optical waveguides," Rev. Mod. Phys. **51**, 341–367 (1979).
21. M. Plöschner, T. Tyc, and T. Čižmár, "Seeing through chaos in multimode fibres," Nat. Photonics **9** (2015).
22. D. E. B. Flaes, J. Stopka, S. Turtaev, J. F. de Boer, T. Tyc, and T. Čižmár, "Robustness of light-transport processes to bending deformations in graded-index multimode waveguides," Phys. Rev. Lett. **120**, 233901 (2018).
23. J. W. Nicholson, A. D. Yablon, S. Ramachandran, and S. Ghalmi, "Spatially and spectrally resolved imaging of modal content in large-mode-area fibers," Opt. Express **16**, 7233–7243 (2008).
24. D. N. Schimpf, R. A. Barankov, and S. Ramachandran, "Cross-correlated (C2) imaging of fiber and waveguide modes," Opt. Express **19**, 13008–13019 (2011).
25. M.-J. Sun, M. P. Edgar, G. M. Gibson, B. Sun, N. Radwell, R. Lamb, and M. J. Padgett, "Single-pixel three-dimensional imaging with time-based depth resolution," Nat. Commun. **7**, 12010 (2016).
26. G. A. Howland, D. J. Lum, M. R. Ware, and J. C. Howell, "Photon counting compressive depth mapping," Opt. Express **21**, 23822–23837 (2013).
27. W. K. Pratt, J. Kane, and H. C. Andrews, "Hadamard transform image coding," Proc. IEEE **57**, 58–68 (1969).
28. Z. Zhang, X. Wang, G. Zheng, and J. Zhong, "Hadamard single-pixel imaging versus fourier single-pixel imaging," Opt. Express **25**, 19619–19639 (2017).
29. G. Ghosh, "Sellmeier coefficients and dispersion of thermo-optic coefficients for some optical glasses," Appl. Opt. **36**, 1540–1546 (1997).
30. L. Allen, M. W. Beijersbergen, R. J. C. Spreeuw, and J. P. Woerdman, "Orbital angular momentum of light and the transformation of Laguerre-Gaussian laser modes," Phys. Rev. A **45**, 8185–8189 (1992).
31. M. J. Padgett, F. M. Miatto, M. P. J. Lavery, A. Zeilinger, and R. W. Boyd, "Divergence of an orbital-angular-momentum-carrying beam upon propagation," New J. Phys. **17**, 023011 (2015).
32. P. Gregg, P. Kristensen, and S. Ramachandran, "Conservation of orbital angular momentum in air-core optical fibers," Optica **2**, 267–270 (2015).
33. P. Gregg, P. Kristensen, and S. Ramachandran, "13.4km OAM state propagation by recirculating fiber loop," Opt. Express **24**, 18938–18947 (2016).
34. S. Ramachandran and P. Kristensen, "Optical vortices in fiber," Nanophotonics **2**, 455–474 (2013).
35. R. H. Hadfield, "Single-photon detectors for optical quantum information applications," Nat. Photonics **3** (2009).
36. J. Wu, L. You, S. Chen, H. Li, Y. He, C. Lv, Z. Wang, and X. Xie, "Improving the timing jitter of a superconducting nanowire single-photon detection system," Appl. Opt. **56**, 2195–2200 (2017).
37. M.-J. Sun, M. P. Edgar, D. B. Phillips, G. M. Gibson, and M. J. Padgett, "Improving the signal-to-noise ratio of single-pixel imaging using digital microscanning," Opt. Express **24**, 10476–10485 (2016).